Research in Astronomy and Astrophysics, 23:095026 (19pp), 2023 September https://doi.org/10.1088/1674-4527/aceccb
© 2023. National Astronomical Observatories, CAS and IOP Publishing Ltd. Printed in China and the U.K.

Do Minor Interactions Trigger Star Formation in Galaxy Pairs?

Apashanka Das[1], Biswajit Pandey[1], and Suman Sarkar[2,3]
[1] Department of Physics, Visva-Bharati University, Santiniketan, Birbhum, 731235, India; a.das.cosmo@gmail.com, biswap@visva-bharati.ac.in
[2] Department of Physics, Indian Institute of Science Education and Research Tirupati, Tirupati, 517507, India; suman2reach@gmail.com
[3] Department of Physics, Indian Institute of Technology Kharagpur, Kharagpur, 721302, India
Received 2023 March 16; revised 2023 July 22; accepted 2023 July 26; published 2023 September 4

Abstract

We analyze the galaxy pairs in a set of volume limited samples from the Sloan Digital Sky Survey to study the effects of minor interactions on the star formation rate (SFR) and color of galaxies. We carefully design control samples of isolated galaxies by matching the stellar mass and redshift of the minor pairs. The SFR distributions and color distributions in the minor pairs differ from their controls at >99% significance level. We also simultaneously match the control galaxies in stellar mass, redshift and local density to assess the role of the environment. The null hypothesis can be rejected at >99% confidence level even after matching the environment. Our analysis shows a quenching in the minor pairs where the degree of quenching decreases with the increasing pair separation and plateaus beyond 50 kpc. We also prepare a sample of minor pairs with H_α line information. We calculate the SFR of these galaxies using the H_α line and repeat our analysis. We observe a quenching in the H_α sample too. We find that the majority of the minor pairs are quiescent systems that could be quenched due to minor interactions. Combining data from the Galaxy Zoo and Galaxy Zoo 2, we find that only ∼1% galaxies have a dominant bulge, 4%–7% galaxies host a bar and 5%–10% of galaxies show active galactic nucleus (AGN) activity in minor pairs. This indicates that the presence of bulge, bar or AGN activity plays an insignificant role in quenching the galaxies in minor pairs. The more massive companion satisfies the criteria for mass quenching in most of the minor pairs. We propose that the stripping and starvation likely caused the quenching in the less massive companion at a later stage of evolution.

Key words: methods: statistical – galaxies: formation – methods: data analysis – galaxies: interactions – galaxies: star formation – (cosmology:) large-scale structure of universe

1. Introduction

The formation and evolution of galaxies in the Universe remain one of the most challenging problems in modern cosmology. The ΛCDM model is quite successful in explaining most of the cosmological observations on large-scales. However, our understanding of the details of galaxy formation and evolution within the framework of the ΛCDM model is still incomplete. The first bound objects formed in the Universe when the primordial density fluctuations in the dark matter density field collapsed into dark matter halos. Galaxies are believed to have formed by the accretion of neutral hydrogen gas onto the dark matter halos and the subsequent cooling and condensation of the gas at the centers of these halos (Rees & Ostriker 1977; Silk 1977; White & Rees 1978; Fall & Efstathiou 1980).

Galaxies are not island Universes that evolve in isolation. They are an integral part of an extensive and complex network, namely the cosmic web (Bond et al. 1996). The initial conditions at the location of formation, assembly history and interactions with the environment may play crucial roles in the formation and evolution of a galaxy. In the hierarchical scenario, the galaxy interactions and mergers provide an efficient mechanism for the buildup of massive galaxies. Such processes can modify the mass distribution, morphology and star formation activity in these galaxies. Using simulations of tidal interactions, Toomre & Toomre (1972) first showed that spiral and irregular galaxies could transform into ellipticals and S0 galaxies. Subsequent studies with more sophisticated simulations (Barnes & Hernquist 1996; Mihos & Hernquist 1996; Tissera et al. 2002; Cox et al. 2006; Di Matteo et al. 2007; Montuori et al. 2010; Rupke et al. 2010; Torrey et al. 2012; Renaud et al. 2014) revealed that the tidal torques generated during an encounter can trigger starbursts in the interacting galaxies. The efficiency of tidally triggered star formation is known to depend on several factors such as the amount of available gas, depth of the potential well, morphology orbital parameters and internal dynamical properties of the galaxies (Barnes & Hernquist 1996; Tissera 2000; Perez et al. 2006).

The first observational evidence of enhanced star formation in interacting galaxies came from a seminal study on optical colors in morphologically disturbed galaxies by Larson & Tinsley (1978). Subsequently, many other studies on

interacting galaxy pairs from modern spectroscopic redshift surveys confirmed the star formation rate (SFR) enhancement at smaller pair separations (Barton et al. 2000, 2007; Alonso et al. 2004, 2006; Nikolic et al. 2004; Woods et al. 2006, 2010; Woods & Geller 2007; Ellison et al. 2008, 2010; Lambas et al. 2008; Heiderman et al. 2009; Knapen & James 2009; Robaina et al. 2009; Patton et al. 2011; Pan et al. 2018; Das et al. 2023). The level of enhancement reported in most of these studies is within a factor of two compared to isolated galaxies. The enhancement is known to depend on multiple factors such as the separation, luminosity or mass ratio and the type of galaxies involved in the interaction. The changes in star formation are very often studied as a function of the projected separation because it is believed to be an indicator of the merger phase of a galaxy pair. The pairs at smaller separation are most likely undergoing a close passage. On the other hand, the pairs at larger separation may be approaching each other or receding away after their first pericentric passage. Nevertheless, these are difficult to confirm as the projected separation corresponds to a snapshot view of the interaction that does not provide any direct information about the timescale.

The equilibrium model (Dekel et al. 2009; Bouché et al. 2010; Davé et al. 2011, 2012; Lilly et al. 2013) emerged as a successful model of galaxy evolution over the last decade. The model suggests that the galaxies maintain an equilibrium between inflow, outflow and star formation. The galaxies are perturbed off the equilibrium relations by interactions and mergers. These galaxies tend to be driven back toward equilibrium. The deviations in SFR from the equilibrium relation are correlated with the available gas fraction. So, the SFR of a galaxy is primarily decided by the available gas mass, which itself is modulated by inflows and outflows of gas. Moreover, both the fraction of molecular gas in the cold interstellar medium (ISM) reservoir and the rate of conversion of molecular gas to stars are also important (Saintonge & Catinella 2022). Saintonge et al. (2012) demonstrate that the global SFR is driven by both the molecular gas density and gas depletion time. The molecular gas properties may be also affected by galaxy interactions. Pan et al. (2018) find that interactions modify the molecular gas properties in galaxy pairs where the magnitude of the effect is sensitive to the pair configuration. Ellison et al. (2018) study the atomic hydrogen gas fraction in post-merger galaxies and find that the enhanced atomic gas fractions in post-mergers are not a consequence of the merger induced starbursts or outflows but arise due to the enhanced turbulence that decreases the star formation efficiency. Thorp et al. (2022) investigate merger induced starbursts using the ALMaQUEST survey and find that the star formation in some mergers is driven by the abundance of molecular gas fuel whereas the star formation efficiency plays a leading role in others. Violino et al. (2018) examine the relation between star formation and molecular gas properties in galaxy mergers and find that both interactions and internal processes may lead to molecular gas enhancement and decreased depletion times. All these studies suggest that the available gas mass plays a crucial role for star formation in galaxies. However, the galaxies are diverse in their details and star formation in interacting galaxies also depends on the properties of the interacting pairs. Many of these findings are also supported by parsec-scale galaxy-merger simulations (Renaud et al. 2014; Moreno et al. 2021) and analysis of galaxy pairs from hydrodynamical simulations (Patton et al. 2020).

The simulations of galaxy interactions suggest that tidally triggered star formation is more efficient in galaxy pairs with similar stellar mass or luminosity. Such interactions are known as major interactions. On the other hand, minor interactions are the interactions between galaxies with a relatively larger mass or luminosity ratio. Such minor interactions and mergers are expected to be more frequent in a galaxy's history since the frequency of mergers of dark matter halos increases with their mass ratio (Lacey & Cole 1993; Fakhouri & Ma 2008). Studies with simulations (Mihos & Hernquist 1994; Mastropietro et al. 2005; Cox et al. 2008) indicate that a lower level of star formation enhancement may also occur in minor mergers after several billion years.

Most of the observational studies of galaxy pairs confirm the tidally triggered star formation in major interactions. However, the issue of star formation enhancement in minor interactions is less clear. In the hierarchical galaxy formation model (Diaferio et al. 1999; Kauffmann et al. 1999a, 1999b; Somerville & Primack 1999), most interactions and mergers occur between unequal-mass systems due to the greater abundance of low mass and low luminosity galaxies. The minor interactions may thus play a crucial role in galaxy evolution. Any observational study of minor interactions and mergers is challenging due to several reasons. The number of minor pairs identified from magnitude limited surveys are far less than the number of major pairs as the galaxies have similar magnitudes in such surveys. It is also difficult to identify the low-luminosity companions around the more luminous members due to contaminations from the background galaxies. Despite these limitations, the effects of minor interactions on star formation have drawn considerable interest. Lambas et al. (2008) investigate the star formation enhancement in paired galaxies using Two-degree-Field Galaxy Redshift Survey (2dFGRS) and find a dependence on the relative luminosity of the pairs. Nikolic et al. (2004) use the Sloan Digital Sky Survey (SDSS) to analyze star formation in paired galaxies and find no dependence on the luminosity of the companion galaxy. Woods et al. (2006) analyze data from the CfA2 survey and a follow-up search to find that the star formation enhancement in pairs decreases with increasing stellar mass ratio. Woods & Geller (2007) show that the specific SFR of the less massive member in a minor pair is enhanced, whereas the more massive member remains unaffected. Ellison et al. (2008) analyze SDSS data and find tentative evidence for higher SFR for the less massive companions in minor pairs at a low significance level. Li

et al. (2008) also reach a similar conclusion using SDSS data. Our current understanding of the impact of minor interactions and mergers is far from complete. The observational studies do not provide conclusive evidence of enhanced star formation in minor pairs in the present Universe.

SDSS (Strauss et al. 2002) is the largest photometric and spectroscopic redshift survey available at present. The availability of precise spectroscopic information for a large number of galaxies in the SDSS provides an excellent opportunity for the statistical study of minor interactions and their effects on star formation and color. We intend to study the SFR and color of minor galaxy pairs in the present Universe using SDSS.

A galaxy's color is strongly correlated with its star formation due to the observed bimodality (Strateva et al. 2001; Baldry et al. 2004; Pandey 2020). The galaxies in the blue cloud are gas rich and they have higher SFRs. Contrarily, the red sequence hosts gas poor galaxies with very low to no star formation. The tidal interactions and mergers between galaxies may trigger starbursts or quenching which consequently alters their colors. Such color changes usually happen on a timescale longer than the starburst or quenching. The effect of tidal interactions on the galaxy pairs can be captured more convincingly if we employ both SFR and color for such studies. We plan to study the SFR and the dust corrected $(u-r)$ color of minor galaxy pairs in a set of volume limited samples from the SDSS and compare these with the respective control samples of the isolated galaxies.

The outline of the paper is as follows. We describe the data and the method of analysis in Section 2, discuss the results in Section 3 and present our conclusions in Section 4.

Throughout the paper we use the ΛCDM cosmological model with $\Omega_{m0}=0.315$, $\Omega_{\Lambda 0}=0.685$ and $h=0.674$ (Planck Collaboration et al. 2018) for conversion of redshift to comoving distance.

2. Data and Method of Analysis

2.1. SDSS DR16

The SDSS is a multi-band imaging and spectroscopic redshift survey with a 2.5 m telescope at Apache Point Observatory in New Mexico. The technical details of the SDSS telescope are described in Gunn et al. (2006) and a description of the SDSS photometric camera can be found in Gunn et al. (1998). The selection algorithm for the SDSS main galaxy sample is discussed in Strauss et al. (2002) and a technical summary of the survey is provided in York et al. (2000).

We use the sixteenth data release (DR16) of the SDSS to identify the galaxy pairs in the nearby Universe. We employ structured query language to download the spectroscopic and photometric information on galaxies in DR16 (Ahumada et al. 2020) from the SDSS CasJobs.[4] We select a contiguous region of the sky that spans $135^\circ \leqslant \alpha \leqslant 225^\circ$ and $0^\circ \leqslant \delta \leqslant 60^\circ$ in equatorial coordinates. We consider all the galaxies with r band Petrosian magnitudes $m_r \leqslant 17.77$ and construct three volume limited samples by restricting the r band absolute magnitude to $M_r \leqslant -19$, $M_r \leqslant -20$ and $M_r \leqslant -21$. The details of these samples are provided in Table 1. The three magnitude bins are not independent of each other. We also try to construct pair samples using independent magnitude bins. However this drastically reduces the number of available minor pairs. The primary motivation behind the choice of these magnitude bins is to investigate if there is any luminosity dependence on the outcomes of minor interactions.

Table 1
This Table Lists the Total Number of Galaxies, the Number of Available Pairs, and the Number of Paired and Isolated Galaxies in the three Volume Limited Samples Considered in this Work

Volume Limited Sample	$M_r \leqslant -19$ ($z \leqslant 0.0422$)	$M_r \leqslant -20$ ($z \leqslant 0.0752$)	$M_r \leqslant -21$ ($z \leqslant 0.1137$)
Number of galaxies	21 984	69 456	85 745
Number of pairs	2581	5441	3039
Number of paired galaxies	4032	9389	5679
Number of isolated galaxies	17,952	60,067	80,066

Note. The number of paired galaxies are not exactly twice the number of pairs as we allow a single galaxy to be part of multiple pairs provided they satisfy the pair selection criteria.

We obtain the stellar mass and SFR of the galaxies from the *StellarMassFSPSGranWideNoDust* table. These are calculated using the Flexible Stellar Population Synthesis (FSPS) model (Conroy et al. 2009). We retrieve information on internal reddening $E(B-V)$ of the galaxies from the *emmissionLinesPort* table which is based on publicly available Gas AND Absorption Line Fitting (GANDALF, Sarzi et al. 2006) and Penalised Pixel-Fitting (Cappellari & Emsellem 2004). We correct for the dust attenuation in the source galaxy by using its internal reddening $E(B-V)$. While downloading the above information, we consider only those galaxies which have their *scienceprimary* flag set to 1. This ensures that only the galaxies with high quality spectra are used in our analysis. Further, we obtain morphological information on the galaxies in three volume limited samples by cross-matching their *SpecObjID* with the galaxies in Galaxy Zoo (Lintott et al. 2008). We identify elliptical and spiral galaxies, respectively, as those which have their elliptical and spiral debiased vote fraction >0.8. We also obtain information about the presence of a dominant bulge and a bar in the galaxies in our sample by cross-matching their *SpecObjID* with the galaxies in Galaxy Zoo 2 (Willett et al. 2013). We also identify the paired galaxies with an active galactic nucleus (AGN) by cross-matching their *SpecObjID* with the galaxies present in the MPA-JHU spectroscopic catalog (Kauffmann et al. 2003b; Brinchmann et al. 2004).

[4] https://skyserver.sdss.org/casjobs/

2.2. Identification of Galaxy Pairs

We identify the galaxy pairs using the traditional method based on application of simultaneous cuts on the projected separation and the velocity difference.

We calculate the projected separation (r_p) between any two galaxies in the distribution using the following relation,

$$r_p = R\,\theta, \tag{1}$$

where R represents the mean distance of the galaxy pair from the observer given by,

$$R = \frac{c}{2H_0}\left\{\int_0^{z_1}\frac{dz}{E(z)} + \int_0^{z_2}\frac{dz}{E(z)}\right\}. \tag{2}$$

Here c and H_0 carry their usual meaning and $E(z)$, in terms of Ω_{m0}, $\Omega_{\Lambda 0}$ and redshift z, is given by the following relation,

$$E(z) = \sqrt{\Omega_{m0}(1+z)^3 + \Omega_{\Lambda 0}}. \tag{3}$$

The angular separation θ between the two galaxies is,

$$\theta = \cos^{-1}[\cos\delta_1\cos\delta_2\cos(\alpha_1-\alpha_2) + \sin\delta_1\sin\delta_2]. \tag{4}$$

Here (α_1, δ_1) and (α_2, δ_2) are the equatorial coordinates of the two galaxies considered.

The difference between the rest frame Hubble velocities of the two galaxies is given by,

$$\Delta v = c\left|\frac{z_1}{1+z_1} - \frac{z_2}{1+z_2}\right|. \tag{5}$$

In order to select the galaxy pairs, we impose simultaneous cuts on the projected separation and the velocity difference of the two galaxies under consideration. Any two galaxies are considered to form a pair if their projected separation $r_p < 150$ kpc and the rest frame velocity difference $\Delta v < 300$ km s^{-1}. It is known from earlier studies that the pairs with larger separations are unlikely to be interacting (Patton et al. 2000; De Propris et al. 2007).

An earlier work by Scudder et al. (2012) shows that excluding galaxies with multiple companions does not alter their results. So, we allow a single galaxy to be part of multiple pairs provided they satisfy the criteria imposed on r_p and Δv.

The pair selection algorithm, when applied to the total of 350,536 galaxies from the contiguous region considered in our analysis, yields a total of 24,756 galaxy pairs. We then cross-match the galaxies in the volume limited sample for $M_r \leqslant -19$, $M_r \leqslant -20$ and $M_r \leqslant -21$ with the galaxies in the identified pairs. This provides us with a total of 2581, 5441 and 3039 galaxy pairs present in our volume limited samples corresponding to the three magnitude bins listed in Table 1. We ensure that the matched galaxies in pairs must have measurements of stellar mass, SFR and internal reddening. We then impose another cut so as to only consider the pairs with stellar mass ratio $\leqslant 10$. This restriction reduces the available number of galaxy pairs to 2024, 5014 and 3002 in the three volume limited samples considered in our work.

2.3. SDSS Fiber Collision Effect: Culling Pairs

It is important to take into account spectroscopic incompleteness due to the finite size of the SDSS fibers. The minimum separation of the fiber centers in the SDSS is 55″ (Strauss et al. 2002). Consequently, the companion galaxies closer than 55″ are preferentially missed. This leads to an under-selection of the closer angular pairs. The galaxies within the collision limit can still be observed if they lie in the overlapping regions between adjacent plates. The ratio of spectroscopic to photometric pairs decreases from ∼80% at >55″ to ∼26% at lower angular separation (Patton & Atfield 2008). This incompleteness effect can be compensated by randomly culling 67.5% of galaxies in pairs with the angular separation >55″ (Ellison et al. 2008; Patton et al. 2011; Scudder et al. 2012).

Our three volume limited samples for $M_r \leqslant -19$, $M_r \leqslant -20$ and $M_r \leqslant -21$, respectively, contain 2024, 5014 and 3002 galaxy pairs. In a similar spirit to earlier works, we randomly exclude 67.5% of pairs which have their angular separation $\theta > 55''$ in all the three samples. The total number of galaxy pairs available for further analysis after culling in the three samples are 737, 2203 and 1600, respectively. The galaxy pairs in the three samples before and after culling are depicted in Figure 1.

In the three volume limited samples ($M_r \leqslant -19$, $M_r \leqslant -20$ and $M_r \leqslant -21$), there are, respectively, 17,952, 60,067 and 80,066 (Table 1) galaxies that have no identified pairs according to the criteria applied in Section 2.2. We term these galaxies as isolated and use them to build our control sample as described in the next subsection.

2.4. Building Control Sample

The physical properties of interacting galaxies should be compared against a carefully designed control sample of non-interacting galaxies. The color and SFR of galaxies depend on their stellar mass. So, it is crucial to ensure that the distributions of stellar mass for the pairs and control samples are statistically indistinguishable. The color and star formation activity of galaxies are also known to depend on the redshift. The redshift dependent selection effects cannot be eliminated completely even in a volume limited sample. So, we also decide to match the redshift distributions of the paired galaxies and control sample of isolated galaxies.

After correcting for the fiber collision effect by culling galaxy pairs as described in Section 2.3, we have a total of 737, 2203 and 1600 pairs in the three volume limited samples. We adopt a strategy similar to Ellison et al. (2008) for building the control sample. We build the control sample of the isolated galaxies by simultaneously matching their stellar mass and redshift with those of the paired galaxies. For each paired

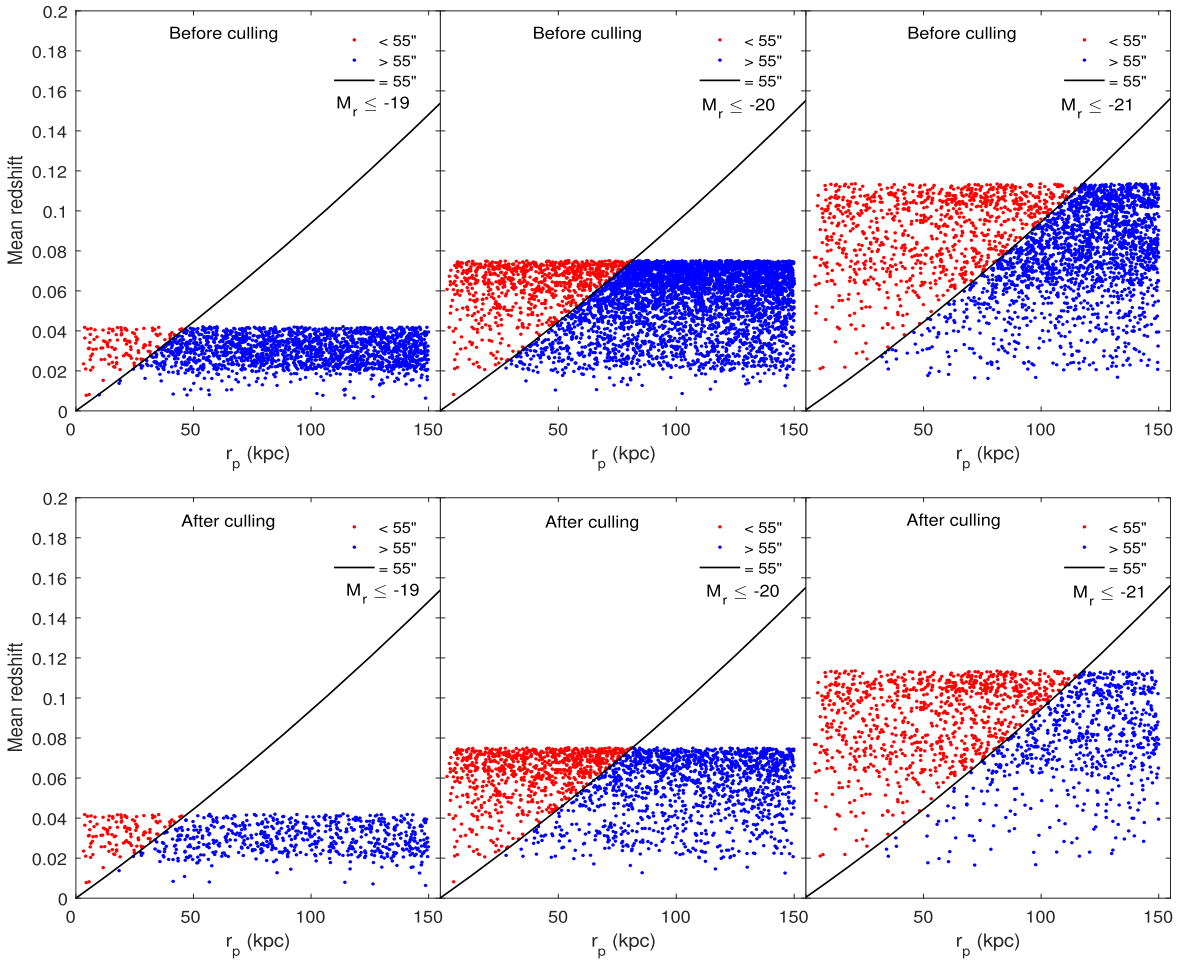

Figure 1. The top panels feature the mean redshift versus the projected separation of pairs before culling in the three volume limited samples. Pairs having angular separation less than 55″ and greater than 55″ are marked using red and blue dots, respectively. The black solid line represents the theoretical curve for angular separation equal to 55″. The bottom panels show the same after culling.

galaxy, we pick five unique isolated galaxies matched in stellar mass and redshift. We match the paired galaxies and their controls within 0.085, 0.050 and 0.061 dex in stellar mass and 0.0065, 0.0010 and 0.0030 in redshift for the three samples corresponding to the magnitude bins $M_r \leqslant -19$, $M_r \leqslant -20$ and $M_r \leqslant -21$, respectively. We match every paired galaxy to their controls and then perform a Kolmogorov–Smirnov (KS) test on the stellar mass and redshift distributions. The probability density functions (PDFs) and cumulative distribution functions (CDFs) of the paired and control matched galaxies are plotted in Figure 2. The results for the corresponding KS tests are tabulated in Table 2. The control samples are accepted only when their stellar mass and redshift distributions are consistent with those of the paired galaxies at a level of at least 30% KS probability for $M_r \leqslant -20$ and 60% KS probability for the remaining two magnitude bins. This implies that the null hypothesis can be rejected at $\leqslant$30% confidence level (Table 2) for $M_r \leqslant -20$ and $\leqslant$60% confidence level (Table 2) for $M_r \leqslant -19$ and $M_r \leqslant -21$. This ensures that the galaxies in the pair and control samples are highly likely to be drawn from the same parent redshift and stellar mass distributions. The two magnitude bins $M_r \leqslant -19$ and $M_r \leqslant -21$ contain relatively smaller numbers of pairs as compared to the magnitude bin $M_r \leqslant -20$. So, a somewhat higher threshold for the confidence level was used to prepare the control samples in these two magnitude bins.

All the paired galaxies in our volume limited samples have measurements of stellar mass and redshift, but the condition that there should be at least five control galaxies for each paired galaxy reduces the number of available galaxy pairs. After the control matching, we have 737, 2159 and 1592 galaxy pairs in the three volume limited samples corresponding to the magnitude bins $M_r \leqslant -19$, $M_r \leqslant -20$ and $M_r \leqslant -21$, respectively. These galaxy pairs are formed by a total of 1363, 4032

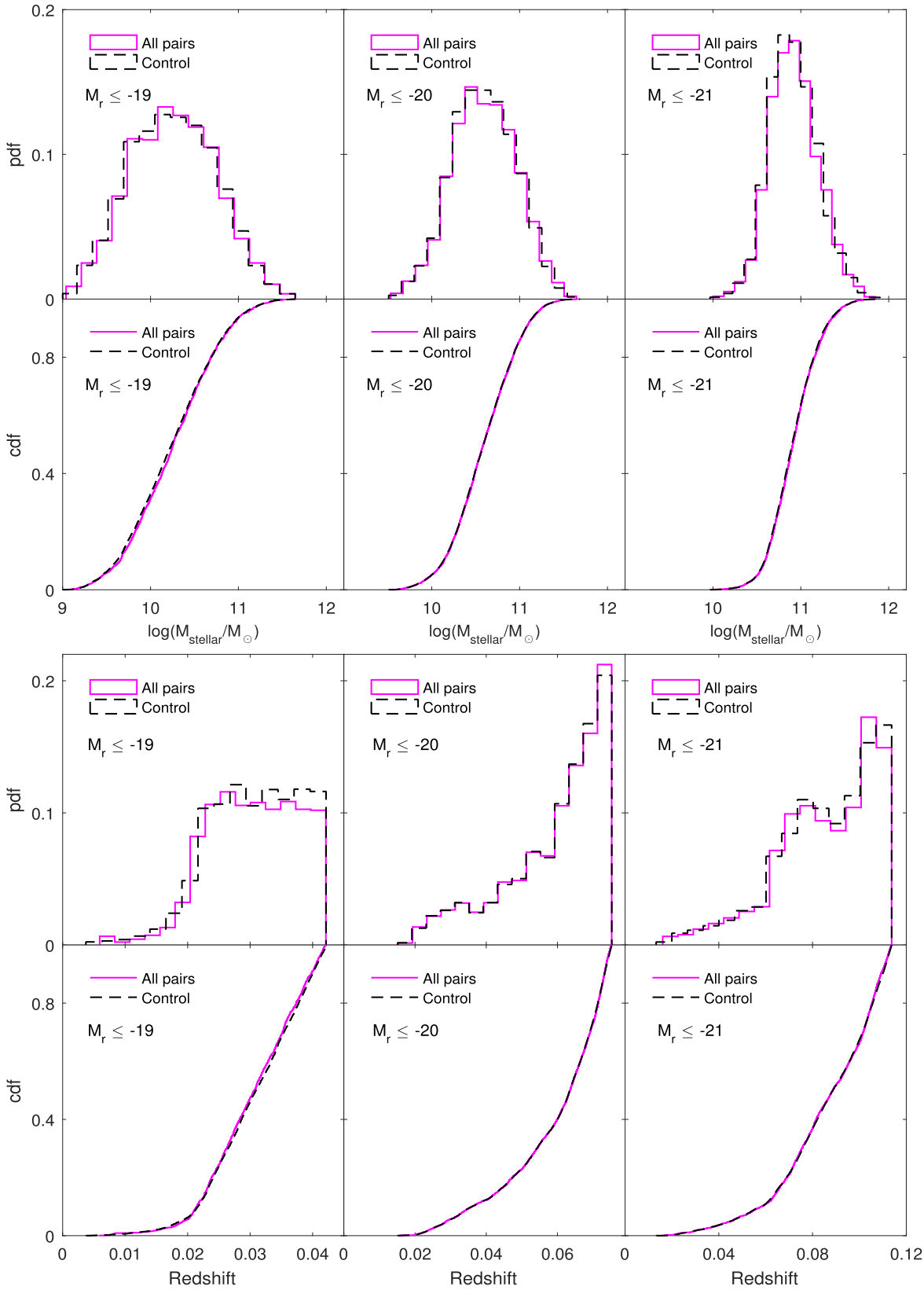

Figure 2. The top two panels, respectively, show PDF and CDF of $\log(M_{\rm stellar}/M_{\rm sun})$ for all pairs and their corresponding control matched isolated galaxies in three absolute magnitude limits $M_r \leqslant -19$, $M_r \leqslant -20$ and $M_r \leqslant -21$. The bottom two panels display the same but for redshift.

Table 2
This Table Lists the Kolmogorov–Smirnov Statistic D_{KS} for Comparisons of Redshift and $\log(M_{stellar}/M_{sun})$ of all Pairs and their Corresponding Control Galaxies in three Volume Limited Samples

	D_{KS}		$D_{KS}(\alpha)$						
M_r	Redshift	$\log(M_{stellar}/M_{sun})$	99%	90%	80%	70%	60%	50%	40%
$\leqslant -19$	0.0267	0.0273	0.0483	0.0363	0.0318	0.0289	0.0266	0.0247	0.0230
$\leqslant -20$	0.0116	0.0123	0.0281	0.0211	0.0185	0.0168	0.0155	0.0144	0.0134
$\leqslant -21$	0.0181	0.0178	0.0322	0.0242	0.0212	0.0192	0.0177	0.0164	0.0153

Note. The table also lists the critical values $D_{KS}(\alpha)$ above which the null hypothesis can be rejected at different confidence levels.

and 3074 galaxies, respectively. The control sample of these paired galaxies consists of a total of 6815, 20,160 and 15,370 isolated galaxies, respectively. The control matching in stellar mass and redshift eliminates most of the biases that can plague a comparison between the two samples (Perez et al. 2009).

We define minor pairs as those which have their stellar mass ratio in the range $3 \leqslant \frac{M_1}{M_2} \leqslant 10$. We find that there are 350, 756 and 338 minor pairs after control matching in the three volume limited samples corresponding to the magnitude bins $M_r \leqslant -19$, $M_r \leqslant -20$ and $M_r \leqslant -21$, respectively. These minor pairs are, respectively, formed by 675, 1479 and 671 galaxies. We note that the minimum projected separation between the galaxies in the minor pairs in all the three volume limited samples is ~4 kpc. We show the image of one representative minor pair from each of the three volume limited samples in Figure 4. The *SpecObjID* and the stellar mass of the member galaxies are provided in each panel of Figure 4.

The environment plays a crucial role in determining a galaxy's properties. The paired galaxies may preferentially reside in high density environments. This may affect any comparison between the color and SFR of the paired galaxies and the isolated galaxies in our sample. To account for this, we also match the local density of the paired and isolated galaxies besides matching their stellar mass and redshift. However, this significantly reduces the number of available minor pairs in our samples. So, we simultaneously match the stellar mass, redshift and local density of paired galaxies and their controls only for the volume limited sample corresponding to the magnitude bin $M_r \leqslant -20$. Here the paired galaxies and their controls are matched within 0.005 in redshift, 0.08 dex in stellar mass and 0.001 in local density (Mpc^{-3}). The PDFs and CDFs of the paired and control matched galaxies are plotted in Figure 3. The results for the corresponding KS tests are tabulated in Table 3. We get a total 1076 pairs after control matching out of which 328 are minor pairs.

We estimate the local number density at the location of each galaxy by using the kth nearest neighbor method (Casertano & Hut 1985). The local number density is defined as,

$$\eta_k = \frac{k-1}{\frac{4}{3}\pi r_k^3}. \quad (6)$$

Here r_k is the distance between the galaxy and its kth nearest neighbor. We choose $k = 5$ for the present analysis.

2.5. Color and SFR Offsets

The ongoing interaction between the galaxies in a pair can influence their color and star formation. The paired galaxies would be bluer compared to the control matched isolated galaxies when SFR is enhanced due to the tidal interaction. However, the color of a galaxy pair can also become redder than the color of its control matched isolated galaxies. This could happen due to the fact that paired galaxies reside in higher density regions than the regions occupied by the control sample of isolated galaxies. This reddening of color is therefore also true for pairs in which interaction between the two members has not started and they are in the stage of pre-interaction (Patton et al. 2011). Such a change in color of the galaxies in a pair and their corresponding control galaxies would not be detected individually and only an overall change could be detected by comparing the color distributions of the entire pair and control samples.

We compute the color offset of every paired galaxy in our sample with respect to its control galaxies. Patton et al. (2011) define the color offset of an individual paired galaxy as the difference between its color and the mean color of its five associated control galaxies. Similarly, the color offset of each control galaxy is defined as the difference between its color and the mean color of the remaining four control galaxies. Following this strategy, we compute the color offset of each galaxy in minor pairs and the corresponding control galaxies in each of the three volume limited samples considered in this work. We then compute the difference between the color offsets of all galaxies in minor pairs and their control galaxies at each projected separation (r_p). We estimate the cumulative mean of this color offset difference Δ ($u-r$ offset) as a function of the projected separation. It can be noted that if the color of paired and control galaxies represents subsets of the same color distribution, then the average value of color offset difference is expected to be zero (Patton et al. 2011).

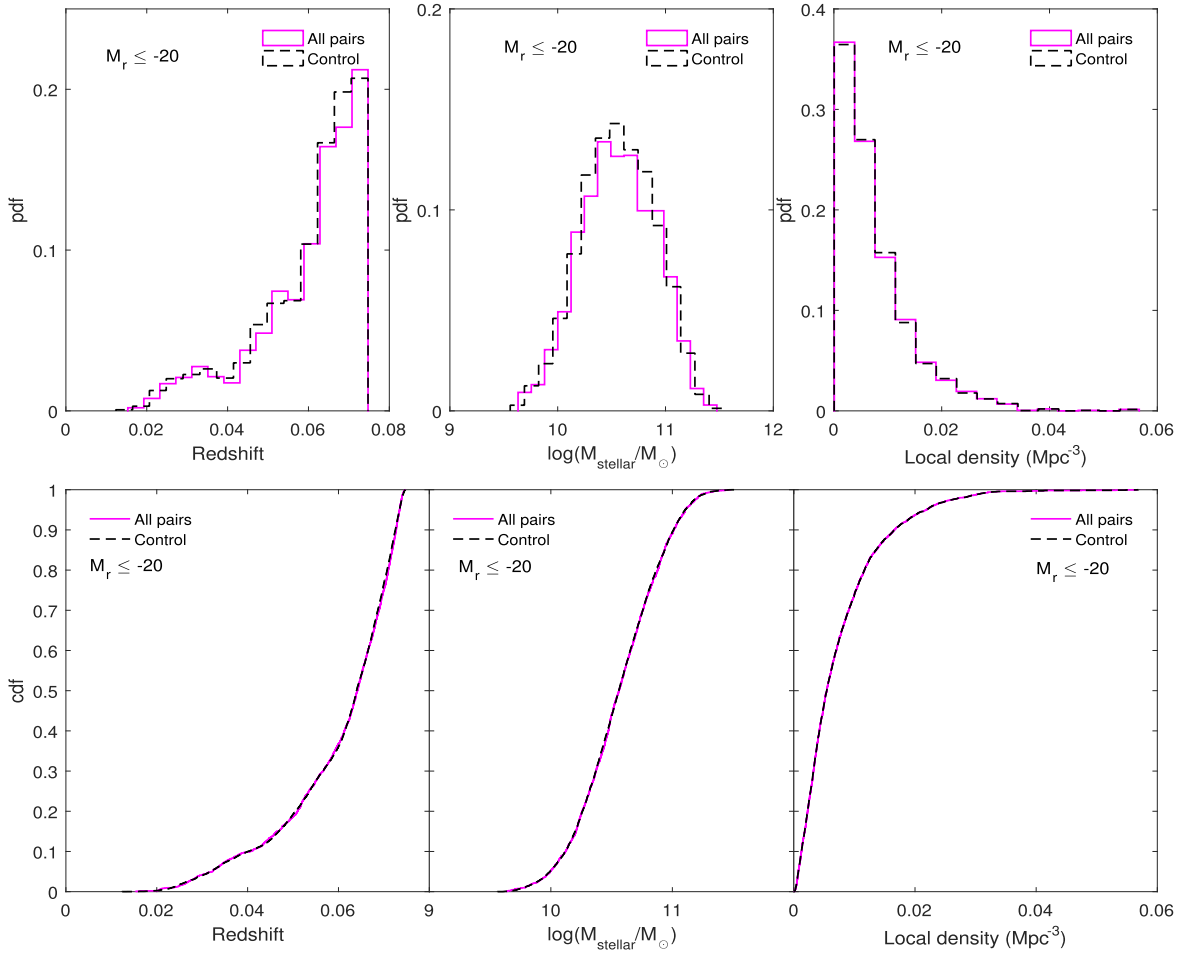

Figure 3. The top panels show the PDF of the redshift, stellar mass and local density of all the paired galaxies and their corresponding control matched isolated galaxies in the volume limited sample corresponding to the magnitude bin $M_r \leqslant -20$. The bottom panels display the respective CDFs.

Table 3
This Table Lists the Kolmogorov–Smirnov Statistic $D_{\rm KS}$ for Comparisons of Redshift, $\log(M_{\rm stellar}/M_{\rm sun})$ and Local Density of all Pairs and their Corresponding Control Galaxies in the Volume Limited Sample Corresponding to the Magnitude Bin $M_r \leqslant -20$

	$D_{\rm KS}$			$D_{\rm KS}(\alpha)$				
M_r	Redshift	$\log(M_{\rm stellar}/M_{\rm sun})$	Local Density	99%	90%	80%	70%	60%
$\leqslant -20$	0.0218	0.0223	0.0205	0.0392	0.0295	0.0258	0.0235	0.0216

Note. The critical values $D_{\rm KS}(\alpha)$ above which the null hypothesis can be rejected at different confidence levels are also listed in the same table.

We also calculate the SFR offset of each galaxy in minor pairs and their corresponding control galaxies in all the volume limited samples in a similar manner. The cumulative mean of the SFR offset difference Δ(SFR offset) is estimated as a function of the projected separation. The Δ(SFR offset) is expected to be positive for SFR enhancement, negative for suppression in SFR and zero when there are no differences in the SFR of the paired galaxies and their controls.

3. Results

3.1. Comparing SFR and (u − r) Color Distributions in the Minor Pairs and the Isolated Galaxies After Matching the Stellar Mass and Redshift

We would like to understand the role of minor interactions on the SFR and color of galaxies in the present Universe. It is important to test whether the galaxies in a minor pair and their control sample of isolated galaxies have any differences in their

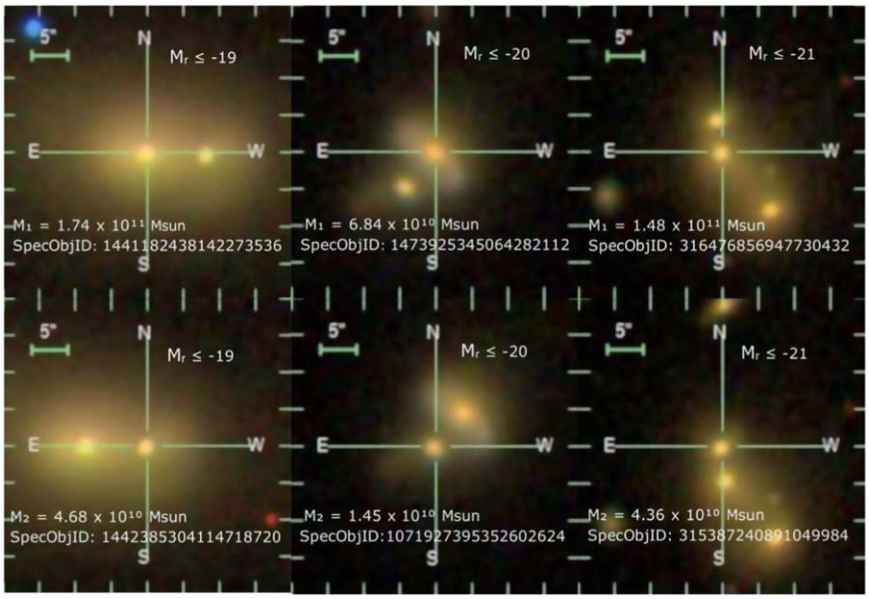

Figure 4. This displays the image of one minor pair from each of the volume limited samples. The more massive and less massive members in the minor pairs are marked in the top and bottom panels, respectively. The stellar mass and SDSS *SpecObjID* of the member galaxies are mentioned separately in each panel.

color and SFR distributions. We compare the $(u-r)$ color distribution of the galaxies in minor pairs and their control samples in three volume limited samples in the top three panels of Figure 5. The galaxies can be divided into blue and red classes by employing a cut in their $(u-r)$ color. The galaxies with $(u-r) < 2.22$ and $(u-r) > 2.22$ can be labeled as blue and red, respectively (Strateva et al. 2001). We find more red galaxies in the minor pairs compared to their control samples in each of the volume limited samples. In addition, the control samples of the isolated galaxies contain a relatively larger number of blue galaxies than the samples of minor pairs. We also compare the CDFs of the $(u-r)$ color for the paired and control galaxies in each volume limited sample in the bottom panels of Figure 5. We perform a KS test to check if the distributions of $(u-r)$ color in minor pairs and their control samples are statistically different in a significant manner. The results of the KS test are tabulated in Table 4 which clearly show that the null hypothesis can be rejected at the >99% confidence level for each volume limited sample. So, the $(u-r)$ color of the minor pairs is significantly different from the galaxies in their control samples.

We perform a similar analysis with the SFR of the galaxies in the minor pairs and their controls. The PDFs and CDFs for the paired and isolated galaxies are compared in the top and bottom panels of Figure 6, respectively. The top panels of Figure 6 affirm that the minor pairs contain a larger number of low star-forming galaxies compared to their control samples in each volume limited sample. Noticeably, the number of high star-forming galaxies in the minor pairs is lower than the respective control samples of the isolated galaxies. The results of the KS test for SFR distributions are also tabulated in Table 4. We find that the SFR of the minor pairs and their controls are significantly different, and the null hypothesis can be rejected at >99% confidence level.

We depict the cumulative mean of the Δ $(u-r$ offset) as a function of projected separation for the three volume limited samples in the top panels of Figure 8. The results confirm that the Δ $(u-r$ offset) is positive at all pair separations up to 150 kpc. The Δ $(u-r$ offset) tends to decrease with increasing pair separation but nearly plateaus beyond 50 kpc in all three volume limited samples. The magnitude of Δ $(u-r$ offset) is relatively higher in the brighter samples. The cumulative mean of the Δ(SFR offset) as a function of projected separation is depicted for all three volume limited samples in the bottom panels of Figure 8. The Δ(SFR offset) is negative throughout the entire pair separation range. The Δ(SFR offset) increases with increasing pair separation up to a distance of $\sim$50 kpc and nearly plateaus out beyond this pair separation. We also note that the magnitude of Δ(SFR offset) is systematically lower for brighter samples. A higher Δ $(u-r$ offset) and lower Δ(SFR offset) for brighter samples indicate a luminosity dependent quenching. Such trends may arise because brighter pairs reside in denser environments where the galaxies are mostly red.

A positive $\Delta(u-r$ offset) indicates that, on average, galaxies in minor pairs are redder than galaxies without a close companion. A negative Δ(SFR offset) corresponds to the suppression of star formation in the minor pairs. So, the trends observed in Δ $(u-r$ offset) and Δ(SFR offset) are consistent. Our results indicate that the minor interactions may initiate quenching in galaxies in the present Universe. However, it is

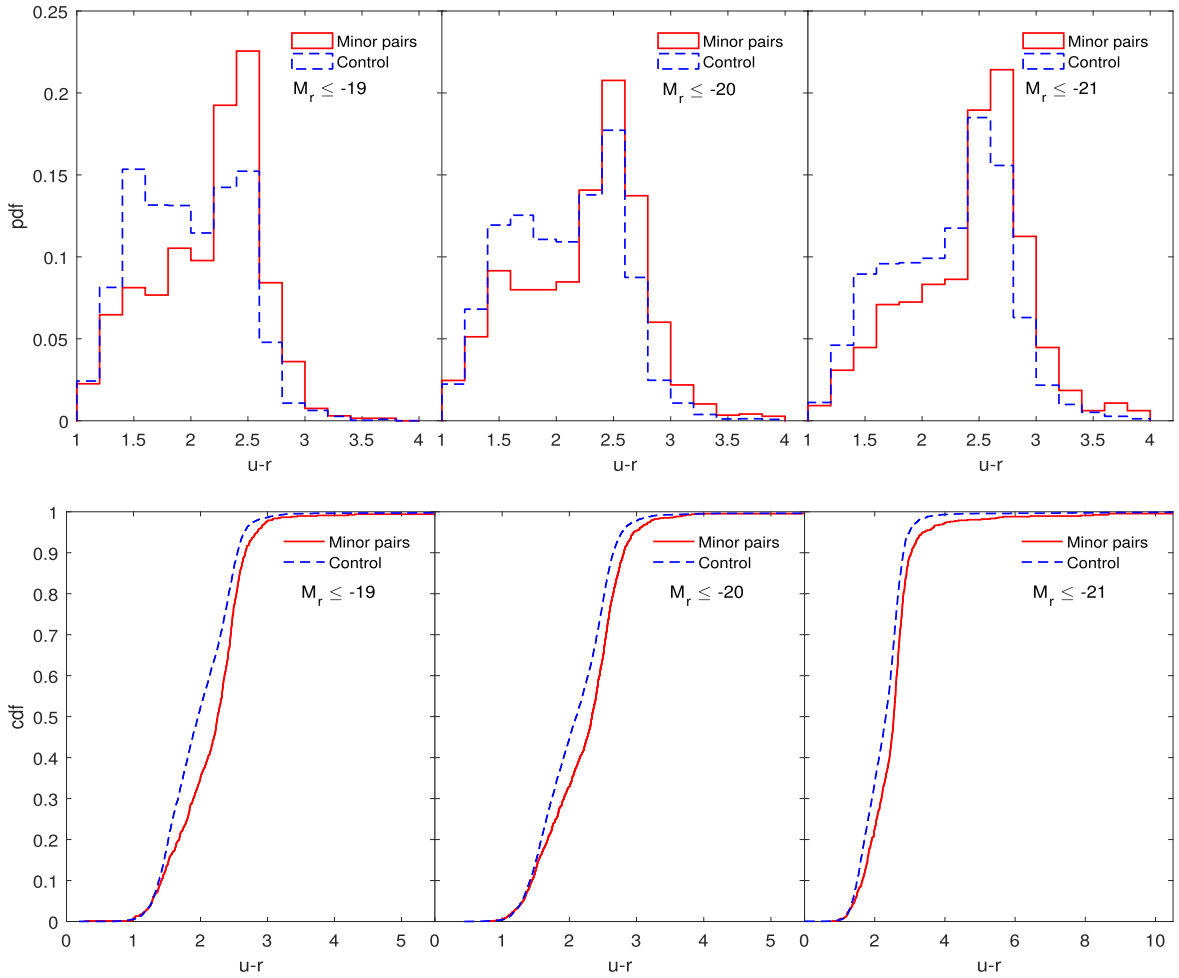

Figure 5. The top and bottom panels, respectively, show the PDF and CDF of $(u - r)$ color of all the minor pairs and their corresponding control matched isolated galaxies in the three volume limited samples.

Table 4

This Table Lists the Kolmogorov–Smirnov Statistic D_{KS} for Comparisons of Star Formation Rate (SFR) and $(u - r)$ Color of Minor Pairs and their Control Galaxies in the three Volume Limited Samples

	D_{KS}		$D_{KS}(\alpha)$							
M_r	SFR	$(u - r)$	99%	90%	80%	70%	60%	50%	40%	30%
$\leqslant -19$	0.1855	0.1944	0.0686	0.0516	0.0452	0.0411	0.0378	0.0351	0.0327	0.0289
$\leqslant -20$	0.1412	0.1481	0.0464	0.0349	0.0306	0.0277	0.0256	0.0237	0.0221	0.0202
$\leqslant -21$	0.1773	0.1908	0.0688	0.0518	0.0454	0.0412	0.0379	0.0352	0.0328	0.0289

Note. The control galaxies are matched in stellar mass and redshift. The table also lists the critical values $D_{KS}(\alpha)$ above which the null hypothesis can be rejected at different confidence levels.

also important to note that the environment may play an important role in such quenching.

The control samples are matched in stellar mass and redshift, which ensure that any differences in the color and SFR distributions of the minor pairs and their controls do not arise due to differences in their stellar mass and redshift distributions. The observed differences in color and SFR may be caused by the differences in their environments. It can be tested by matching the environment of the controls before the comparison.

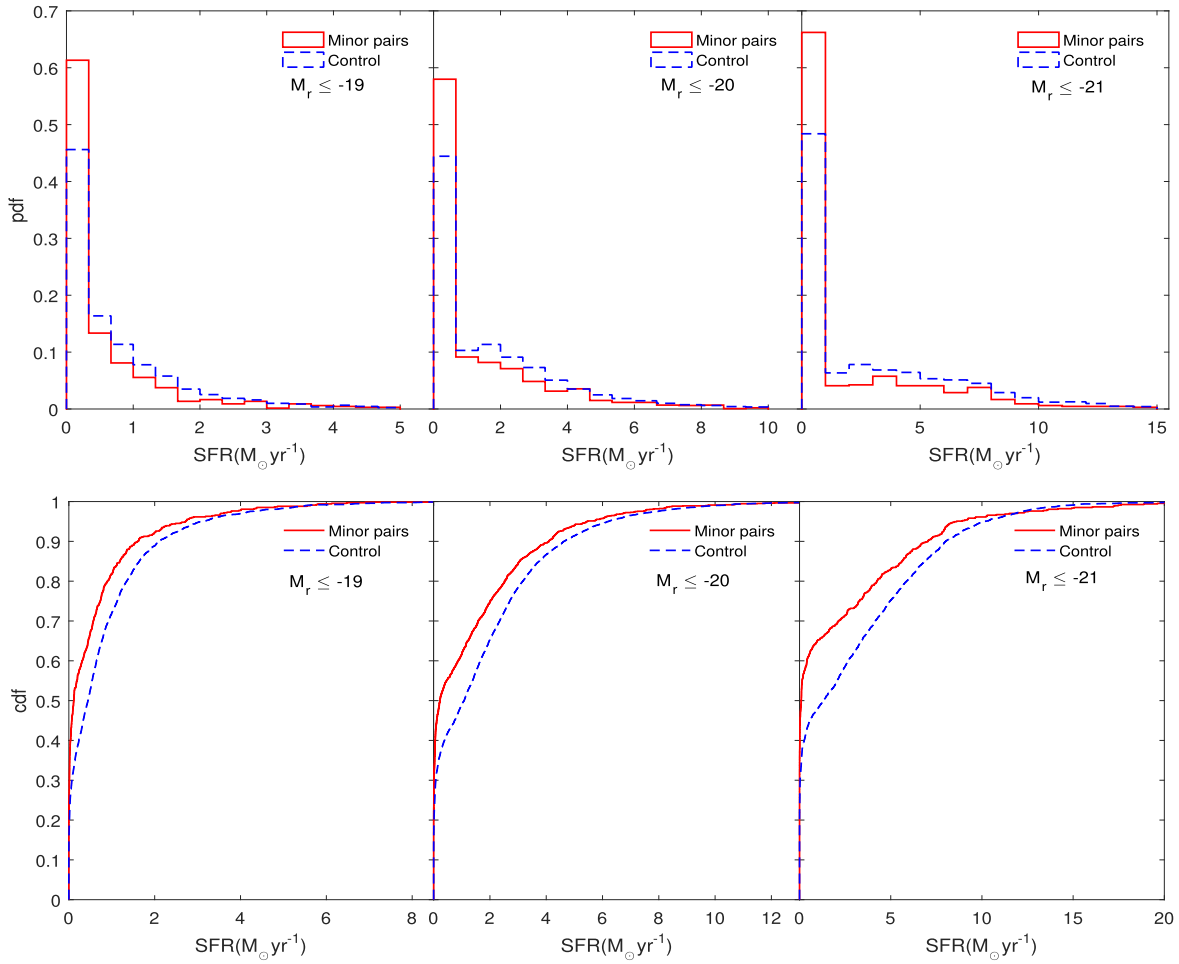

Figure 6. Same as Figure 5, but for the SFR.

3.2. Morphology of the Galaxies in the Minor Pairs

It is well known that the tidal interactions may cause gas loss through AGN or shock-driven winds (Murray et al. 2005; Springel et al. 2005), and induce bar quenching (Haywood et al. 2016) and morphological quenching (Martig et al. 2009). We want to check the bar, dominant bulge and AGN occurrences in the minor pairs. We cross-match the minor pairs with the galaxies in Galaxy Zoo (Lintott et al. 2008) and Galaxy Zoo 2 (Willett et al. 2013) to reveal the morphological properties of the member galaxies in minor pairs. The morphological information on the galaxies in the minor pairs is listed in Table 5. It is worthwhile to mention that the morphological information is not available for ∼50% of the minor pairs in our sample. We examine only the minor pairs for which the morphological information is available. The Spiral–Spiral and Spiral–Elliptical combinations in minor pairs are more prevalent than the Elliptical–Elliptical combination. Only 4%–7% of galaxies in the minor pairs host a bar. A dominant bulge is observed in only ∼1% of the galaxies in the minor pairs; 5%–10% of galaxies in the minor pairs show AGN activity. We observe that only a small percentage of the galaxies in the minor pairs host a bar, dominant bulge or AGN. We do not compare the SFR in minor pairs to that with the galaxies hosting a bar, dominant bulge or AGN. Since the galaxies with an AGN, bar or dominant bulge are known to initiate quenching in galaxies, a dominance of such galaxies in minor pairs would indicate that the observed quenching in minor pairs is primarily driven by these factors. We do not observe any such trends in our analysis.

3.3. Comparing SFR and (u − r) Color Distributions in the Minor Pairs and the Isolated Galaxies After Matching the Stellar Mass, Redshift and Local Density

The quenching in minor pairs may also arise due to the environment. The paired galaxies preferentially reside in denser environments that host redder galaxies. So, the overabundance of red and low star-forming galaxies in the minor pairs compared to their control sample of isolated galaxies may not be caused by

Table 5
This Table Lists Number of the Minor Paired Galaxies that are Classified as Elliptical, Spiral, Uncertain Morphology and those with the Presence of Bar, Dominant Bulge or AGN Activity

	$M_r \leqslant -19$	$M_r \leqslant -20$	$M_r \leqslant -21$
Galaxies in minor pairs after control matching	675	1479	671
Elliptical	147	218	123
Spiral	185	402	160
Uncertain morphology	308	796	351
Morphology not available	35	63	37
Dominant bulge	8	13	6
Bar	24	56	49
AGN	72	98	38
Minor pairs after control matching	350	756	338
Spiral–Spiral	37	66	30
Elliptical–Elliptical	22	13	12
Spiral–Elliptical	34	51	25

Note. It also shows the number of minor pairs with Spiral–Spiral, Elliptical–Elliptical and Spiral–Elliptical combinations.

the interactions alone. One needs to compare these properties by also matching the environment of the control galaxies. We prepare the control samples by simultaneously matching the stellar mass, redshift and local density of the isolated galaxies. We find that such controls can be prepared only for a single volume limited sample ($M_r < -20$) due to the smaller number of minor pairs present in our samples.

We compare the PDFs of $(u - r)$ color and SFR in the minor pairs and their control galaxies in the top two panels of Figure 7. Interestingly, the minor pairs still host more red and low star-forming galaxies compared to their controls. The differences in their PDFs are smaller than those observed in Figures 5 and 6 though. The respective CDFs are compared in the two bottom panels of Figure 7. We perform KS tests to quantify the differences in the distributions of $(u - r)$ color and SFR in the minor pairs and their control galaxies. The results of the KS tests are listed in Table 6 which clearly show that the null hypothesis can still be rejected at >99% confidence level.

We show the cumulative mean of the Δ $(u - r$ offset) and Δ (SFR offset) as a function of pair separation in the two panels of Figure 9. Figure 9 exhibits the same trends as observed in Figure 8. We find that Δ $(u - r$ offset) decreases, and Δ(SFR offset) increases with increasing pair separation. The dependence of the quenching on the pair separation is noticeable at least up to $\sim$50 kpc. The degree of suppression of star formation in minor pairs remains nearly unchanged at greater separations.

The analysis in this subsection implies that the environment has some role in quenching the star formation in minor pairs. Nevertheless, the signature of quenching in minor pairs persists even after controlling for their environment, stellar mass and redshift. It indicates that the minor interaction induces quenching in galaxies in the present Universe.

3.4. Possible Limitations of the Study

We discuss a few limitations of our study in this subsection. It is challenging to obtain reliable photometry in blended systems particularly for low mass galaxies in paired systems. We use the "clean" flag in the SDSS database to check whether the minor merger systems in our samples have reliable photometry. We show the numbers of pairs with clean or unclean photometry as a function of projected separation in the three volume limited samples in Figure 10. There are a small number of minor pairs present in each sample for which both the members have unclean photometry. We see that the relative abundance of such pairs does not depend on their projected separations. Most of the galaxies in minor pairs have clean photometry in our samples. However, the pairs with unclean photometry may have some impact on our results. Considering this, we also repeat our analysis with only the minor pairs with clean photometry and find that our conclusions remain unchanged. The quenching observed in minor pairs in our study is statistical and the trends are identical in all three magnitude bins.

It is also challenging to measure the total flux of each galaxy in the merger systems and calculate the individual SFRs accurately. We use the SFRs derived from a catalog which is based on the stellar population synthesis (SPS) technique (Conroy et al. 2009). The SPS models translate the observations (spectral energy distribution (SED), magnitudes, etc.) to physical properties using a set of fit parameters in the model. We plot the stellar mass versus SFR of the galaxies in minor pairs and their control samples in all three volume limited samples in Figure 11. We find that the galaxies in these samples follow a main sequence relation but with larger scatters at higher masses. This may be related to the substantial uncertainties in the SPS modeling. Such uncertainties may have some impact on our results.

The color is also affected by the reddening or dust extinction in galaxies. The additional reddening is often quantified with the $E(B - V)$ color. It is determined by comparing the observed colors of galaxies with the expected colors of an unreddened stellar population. This color excess affects the intrinsic properties like observed color and SFR of galaxies. A very large reddening for the galaxies in our sample may in principle affect the results of our analysis. We show the color excess $E(B - V)$ versus the observed $(u - r)$ color (without $E(B - V)$ correction) for the minor pairs and their control galaxies in all three volume limited samples in Figure 12. We find that the colors of the minor pairs and their controls are reasonable and

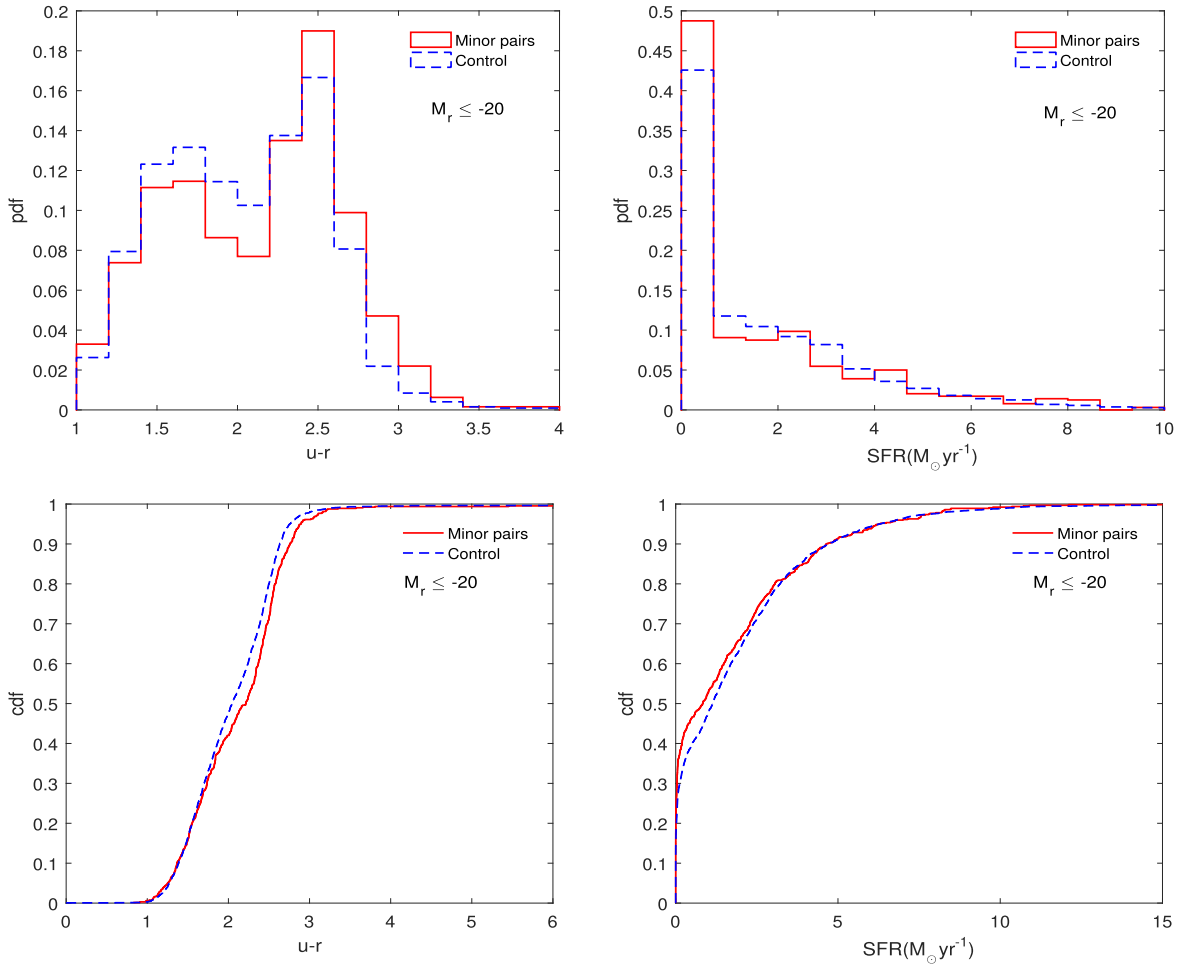

Figure 7. The top left panel of this figure compares the PDF of $(u-r)$ color for the galaxies in minor pairs and their control galaxies matched in stellar mass, local density and redshift. The top right panel compares the same for SFR. The bottom two panels compare the respective CDFs. This figure shows only the results for the volume limited sample corresponding to the magnitude bin $M_r \leqslant -20$.

Table 6
Same as Table 4 but for the Volume Limited Sample Corresponding to the Magnitude bin $M_r \leqslant -20$ and the Control Galaxies that are Matched in Stellar Mass, Redshift and Local Density

	D_{KS}		$D_{KS}(\alpha)$							
M_r	SFR	$(u-r)$	99%	90%	80%	70%	60%	50%	40%	30%
$\leqslant -20$	0.1011	0.0843	0.0702	0.0528	0.0463	0.0420	0.0387	0.0359	0.0335	0.0313

similar in all three samples. We do not expect these to affect our conclusions.

3.5. Roles of Photometric Quality and SFR Estimator

We address these limitations of our study by considering only the galaxies with clean photometry and calculating the SFR of the minor pairs using the H_α line. It is crucial to identify the galaxies having reliable photometry for any analysis with galaxy pairs. Some of the galaxies in our minor pair sample do not have reliable photometry. We only consider the galaxies with reliable photometry by using the "clean" flag in the SDSS database. The brightest magnitude bin in our sample may include some brightest cluster galaxies (BCGs) with their satellites as minor pairs. It shows a higher degree of quenching compared to the other two magnitude bins (Figure 8). The inclusion of BCGs may be responsible for a higher quenching signal in the brightest magnitude bin. Keeping this in mind, we

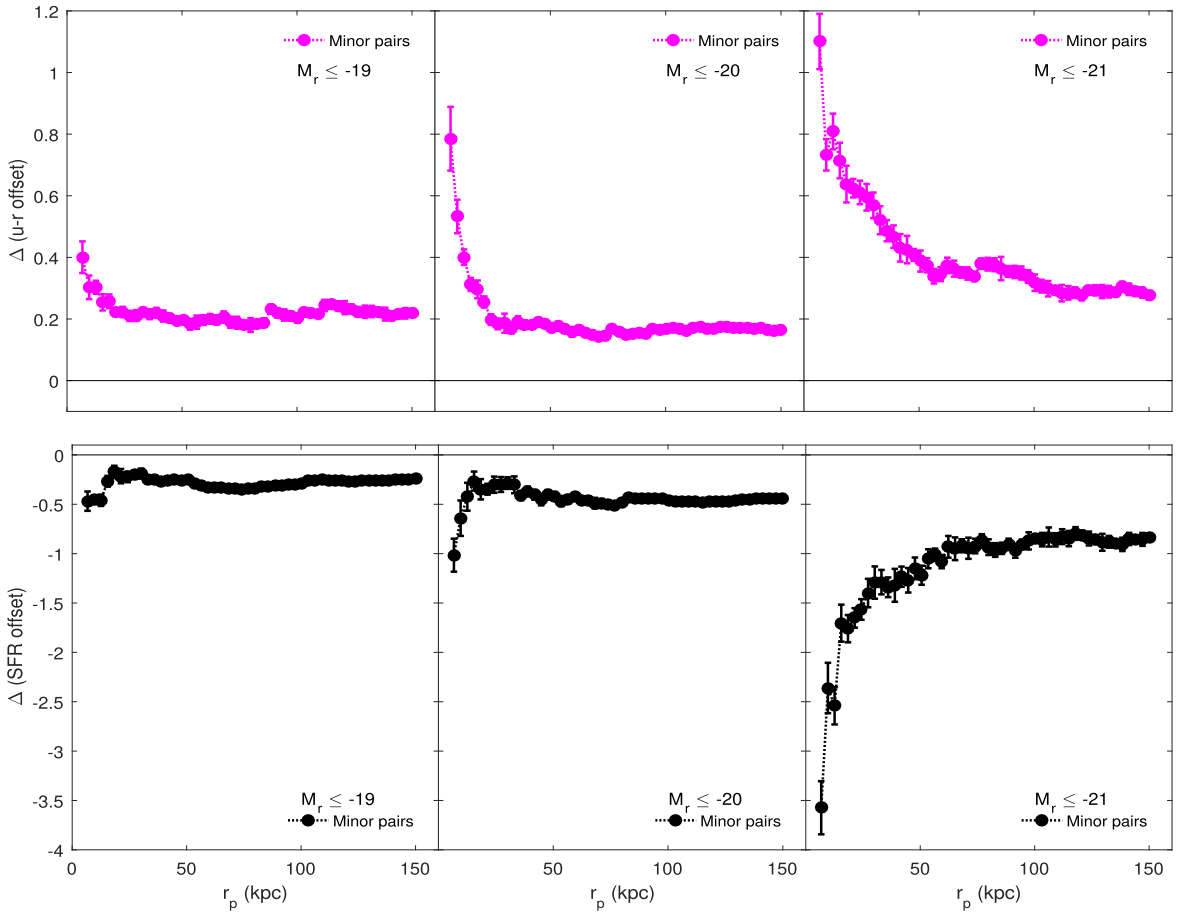

Figure 8. The top and bottom panels, respectively, display the Δ ($u - r$ offset) and Δ(SFR offset) as a function of the projected separation for the three volume limited samples. Here the control galaxies are simultaneously matched in stellar mass and redshift. The 1σ errorbars shown here are estimated using 10 jackknife samples.

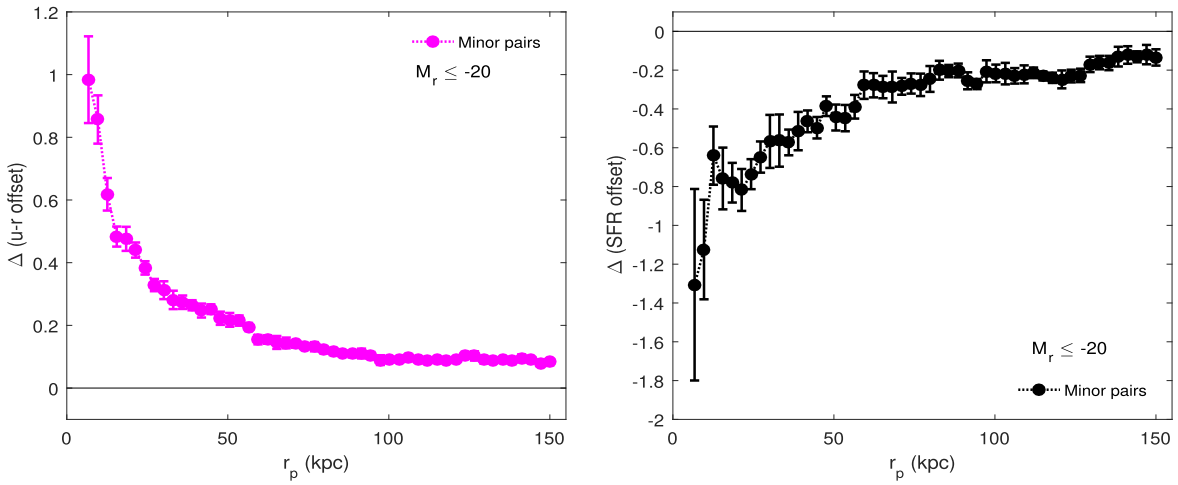

Figure 9. The left and right panels, respectively, show Δ ($u - r$ offset) and Δ(SFR offset) as a function of the projected separation (r_p) for the volume limited sample corresponding to the magnitude bin $M_r \leqslant -20$. Here, we match the control galaxies simultaneously in stellar mass, local density and redshift. The 1σ errorbars displayed here are estimated using 10 jackknife samples.

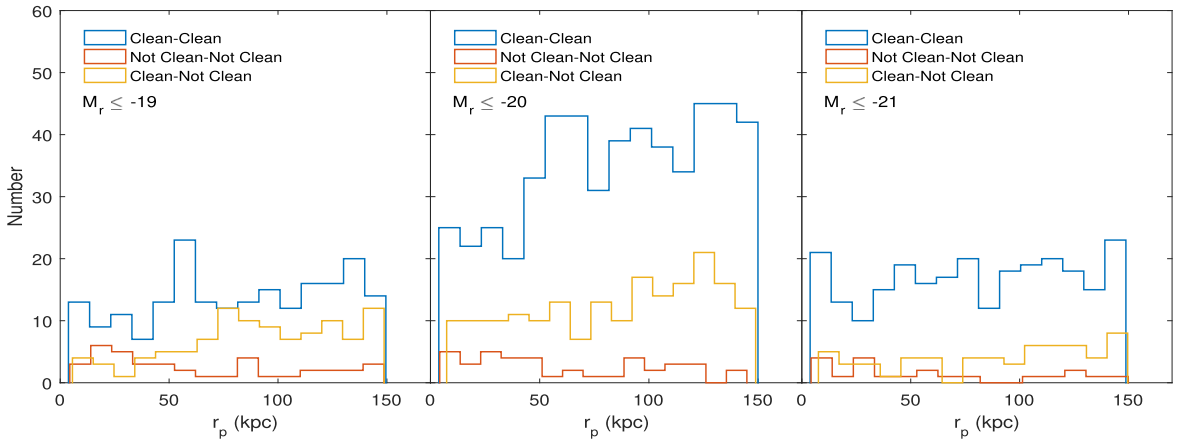

Figure 10. The three panels in this figure show the number of minor pairs with clean/unclean photometry as a function of the projected separations in the three volume limited samples.

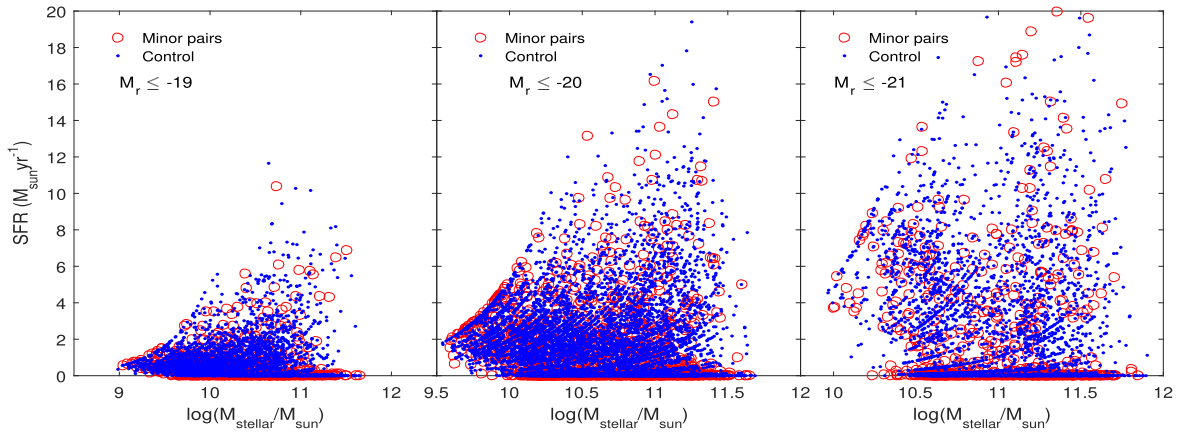

Figure 11. Three panels in this figure show the stellar mass–SFR relation of the minor pairs and their controls in the three volume limited samples.

only repeat our analysis in the faintest magnitude bin ($M_r \leqslant -19$) considered in our analysis. We now have 207 minor pairs in this bin that have clean photometry and H_α line information. The control samples for these minor pairs are obtained following the same method described in Section 2.4.

Our results could be sensitive to different SFR estimators. We calculate the SFR of minor pairs and their control matched sample using the H_α emission line of these galaxies. The SFRs of these galaxies are estimated utilizing the formula (Hopkins et al. 2003),

$$\mathrm{SFR}(M_{\rm sun}\ \mathrm{yr}^{-1}) = 4\pi D_l^2 S_{\mathrm{H}_\alpha} \times \frac{10^{-0.4(r_{\rm petro}-r_{\rm fiber})}}{1.27\times 10^{34}}\left(\frac{S_{\mathrm{H}_\alpha}}{2.86\times S_{\mathrm{H}_\beta}}\right)^{2.114}. \quad (7)$$

Here S_{H_α} and S_{H_β} are stellar absorption corrected H_α and H_β fluxes, respectively. The $r_{\rm petro}$ and $r_{\rm fiber}$ are the Petrosian and fiber magnitudes in the r band of SDSS, respectively, and D_l represents the luminosity distance of the galaxies. The information about the spectral lines of minor pairs and their control matched sample is obtained from the SDSS database by matching their *SpecObjId*s. The cumulative median of the color offset difference and SFR offset difference is plotted as a function of projected separation in Figure 13. The results show a positive value of color offset difference and negative value of SFR offset difference for nearly the entire pair separation range. We find that our results do not change after we discard the galaxies with unreliable photometry and employ a different SFR estimator for our analysis.

4. Conclusions

We study the effects of tidal interactions on the SFR, and the dust corrected $(u-r)$ color of the minor pairs using a set of volume limited samples from the SDSS. We first prepare our control samples by matching the stellar mass and redshift and then compare the SFR and $(u-r)$ color in the minor pairs

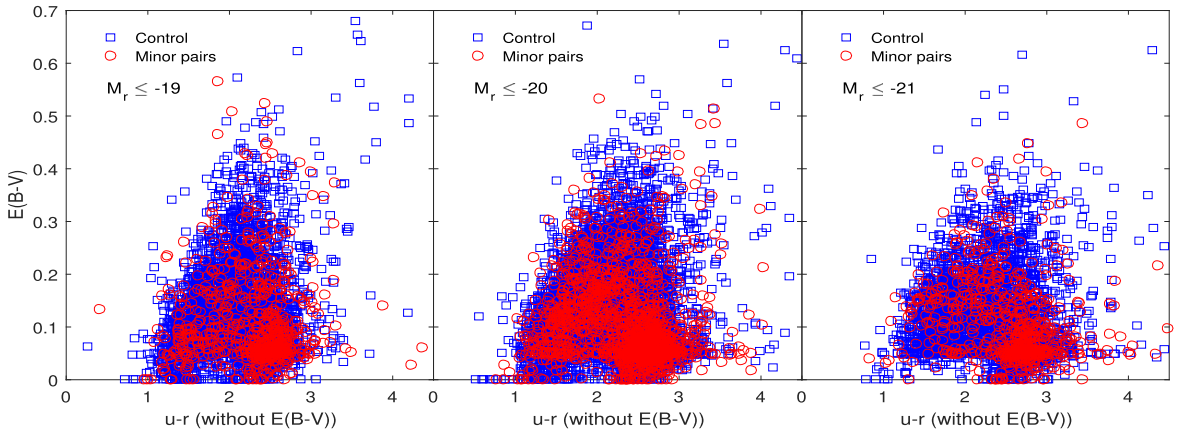

Figure 12. Different panels of this figure display the observed $u-r$ color versus $E(B-V)$ color excess in the three volume limited samples.

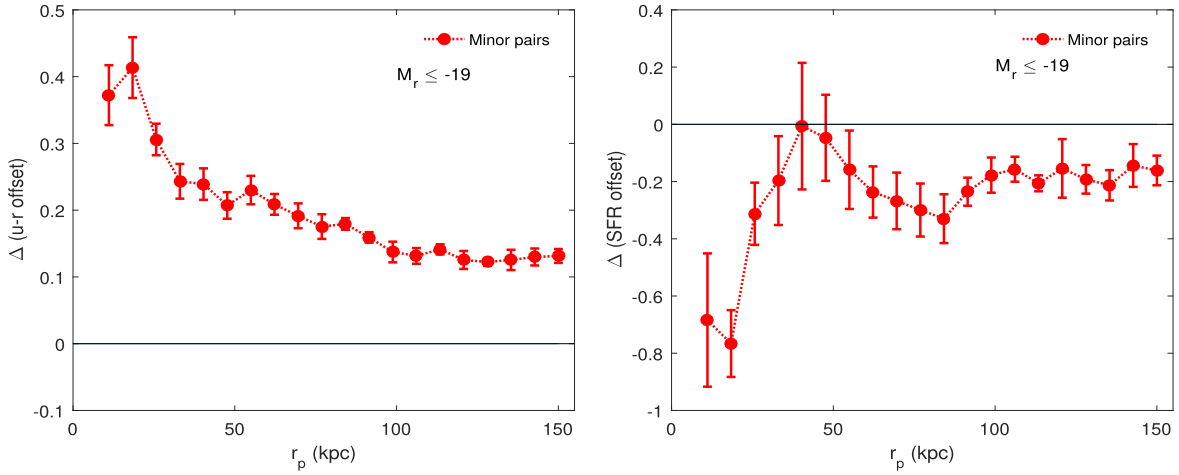

Figure 13. This plot features color offset difference and SFR offset difference of minor pairs having clean photometry in $M_r \leqslant -19$ magnitude bin. Here the SFR of minor pairs and their control matched sample is estimated from the H_α emission line as discussed in Section 3.5.

against their control samples of isolated galaxies. The analysis shows that the SFR and $(u-r)$ color distributions of minor pairs significantly differ from their control galaxies in all three volume limited samples. The null hypothesis can be rejected at >99% confidence level. Both the Δ $(u-r$ offset) and the Δ (SFR offset) as a function of pair separation indicate a quenching in minor pairs. The degree of quenching decreases with increasing pair separation up to ∼50 kpc. The minor pairs in the brighter samples exhibit a higher quenching at a fixed pair separation. The more luminous galaxies preferentially reside in the denser environments where the galaxies are known to be redder. This luminosity dependence indicates some role of the environment in quenching the galaxies in minor pairs.

The control samples of the minor pairs must also be matched in the environment in addition to the stellar mass and redshift. We repeat our analysis with carefully designed control samples that are simultaneously matched in stellar mass, redshift and local density. Interestingly, the SFR and $(u-r)$ color distributions of the minor pairs significantly differ from their control galaxies. The null hypothesis can still be rejected at >99% confidence level. We find that the Δ $(u-r$ offset) and Δ(SFR offset) as a function of pair separation still indicate a quenching in minor pairs even after controlling for their environment. The degree of quenching is sensitive to the pair separation up to ∼50 kpc. Our results suggest that the minor interactions suppress the SFR and enhance the $(u-r)$ color in galaxies. The suppression of the SFR decreases with the increasing pair separation but a non-zero suppression is observed throughout the length scale probed. There is observational evidence that SFR in paired galaxies may be influenced by tidal interactions up to 150 kpc (Scudder et al. 2012; Patton et al. 2013).

The present analysis indicates that the minor interactions suppress the SFR and enhance the $(u-r)$ color in galaxies.

This result seemingly contradicts some of the findings reported in Scudder et al. (2012). This difference most likely arises due to the different treatment of environments. We use the density estimates in three-dimensions incorporating redshift information whereas Scudder et al. (2012) rely on the projected densities for their work. Our pair sample is defined within a volume limited sample whereas the pair sample in Scudder et al. (2012) was defined within a flux limited sample. Most of the selection biases are taken into account in a volume limited sample. The local density can be estimated more reliably within a volume limited sample. We would like to mention here that we indeed observe an enhanced star formation in interacting major pairs (Das et al. 2021, 2023) in our analysis with volume limited samples. However, we observe an opposite trend for the minor pairs.

We also analyze the morphology of the minor pairs by cross-matching the paired galaxies with the Galaxy Zoo and Galaxy Zoo 2. The Spiral–Spiral and Spiral–Elliptical combinations are more frequently observed than the Elliptical–Elliptical combinations in the minor pairs. We note that only $\sim$1% of galaxies have a dominant bulge, 4%–7% of galaxies host a bar and 5%–10% of galaxies manifest AGN activity in the minor pairs. This suggests that the bar, bulge and AGN activity do not take a leading role in quenching the galaxies in the minor pairs.

The minor interactions are believed to trigger a mild enhancement in the star formation activity in the past. However, we do not find such enhancement in the star formation activity in the minor pairs in the local Universe. Our analysis indicates that the minor interactions in the present Universe initiate quenching in galaxies. The degree of quenching decreases with increasing pair separation. A significant number of galaxies in the minor pairs have a stellar mass above $3 \times 10^{10} M_{\odot}$ which are intrinsically redder and less star-forming (Kauffmann et al. 2003a). We propose that the more massive members in the minor pairs may curtail their star formation through mass quenching (Birnboim & Dekel 2003; Binney 2004; Dekel & Birnboim 2006; Das et al. 2021) or major merger-driven quenching (Gabor et al. 2010; Rodríguez Montero et al. 2019). They possibly quench the star formation in their less massive companions at a later stage by stripping away the gas, leading them to starvation (Larson et al. 1980; Somerville & Primack 1999; Kawata & Mulchaey 2008). It should be noted that the control galaxies in our analysis are matched in stellar mass. So, any mass driven quenching would be equally effective in the control matched samples of isolated galaxies. However any quenching induced by the interactions would be present only in the minor paired galaxies.

We carefully select the control galaxies by closely matching the redshift, stellar mass and environment. This approach eliminates the biases in our results. Any other systematic biases should equally affect both the samples and should not be a matter of concern here. However, a few caveats remain in our analysis. All the galaxies in close pairs may not be undergoing interactions. Some pairs may be approaching each other and are yet to experience an encounter. Also some of the selected pairs may not be close in three-dimensional space due to a chance superposition in high-density regions like groups and clusters (Alonso et al. 2004). Nevertheless, these caveats plague all previous analyses of galaxy pairs with observational data.

Any stellar mass incompleteness present in the pair and control samples would spoil the comparisons between their color and SFR. We also apply a stellar mass limit to our volume limited samples and repeat our entire analysis. We find that our conclusions remain unchanged in such an analysis.

We note that some galaxies in our minor pair sample have unreliable photometry. The SFR estimates used in our analysis are derived from the SED fitting. These estimates have large uncertainties at higher stellar masses. We also notice a larger quenching signal for the brightest magnitude bin in our analysis (Figure 8). This indicates that the brightest magnitude bin may contain a significant number of BCGs with their quenched satellite galaxies. Keeping these issues in mind, we select only the galaxies with clean photometry in the faintest magnitude bin. We estimate the SFR of these minor pairs and their control matched sample using the H_{α} line in these galaxies. We repeat our analysis to calculate the SFR and color offsets in the faintest magnitude bin. The results demonstrate that we still obtain a quenching signal in the faintest magnitude bin. This suggests that the quenching phenomenon in minor pairs in our work cannot be explained by the unclean photometry, contaminations from BCGs or differences between the SFR estimators.

Observations indicate that the star formation in galaxies peaked at a redshift of $z \sim 2$–3 (Tran et al. 2010; Förster Schreiber & Wuyts 2020; Gupta et al. 2020). This epoch is often referred to as "cosmic noon." The minor interactions may trigger star formation in galaxies in the early stages of their evolution. The tidal interactions are more effective in inducing star formation during this period due to a lack of stability in the galaxies (Tissera et al. 2002). Minor interactions may have contributed significantly to the rapid rise in cosmic SFR during the "cosmic noon." The cosmic SFR declines sharply between $z = 1$ and $z = 0$ (Madau et al. 1996).

We find that a significant number of minor pairs in our sample have a very low SFR. These quiescent galaxies could be quenched due to multiple reasons. For example, the environment may have some role in such quenching. The presence of a bar, dominant bulge or AGN may also play some role in quenching the galaxies in minor pairs. However, they do not explain the quenching in most minor pairs. We expect the more massive companion to be mass quenched or merger quenched in most minor pairs. We propose that the less massive companion may experience a satellite quenching at a later stage of evolution (van den Bosch et al. 2008; Wright et al. 2022). However, these alternate scenarios cannot be verified in this work and require further studies. The quenching

by minor interactions in the present Universe would contribute significantly to the build-up of the red sequence and the observed bimodality. We propose that this should be taken into account while modeling the observed bimodality.

Acknowledgments

We sincerely thank an anonymous reviewer for the insightful comments and suggestions that helped us to improve the draft. The authors thank the SDSS team for making the data publicly available. B.P. would like to acknowledge financial support from the SERB, DST, Government of India through the project CRG/2019/001110. B.P. would also like to acknowledge IUCAA, Pune for providing support through an associateship program. S.S. acknowledges IISER Tirupati for support through a postdoctoral fellowship.

Funding for the SDSS and SDSS-II has been provided by the Alfred P. Sloan Foundation, the Participating Institutions, the National Science Foundation, the U.S. Department of Energy, the National Aeronautics and Space Administration, the Japanese Monbukagakusho, the Max Planck Society, and the Higher Education Funding Council for England. The SDSS website is http://www.sdss.org/.

The SDSS is managed by the Astrophysical Research Consortium for the Participating Institutions. The Participating Institutions are the American Museum of Natural History, Astrophysical Institute Potsdam, University of Basel, University of Cambridge, Case Western Reserve University, University of Chicago, Drexel University, Fermilab, the Institute for Advanced Study, the Japan Participation Group, Johns Hopkins University, the Joint Institute for Nuclear Astrophysics, the Kavli Institute for Particle Astrophysics and Cosmology, the Korean Scientist Group, the Chinese Academy of Sciences (LAMOST), Los Alamos National Laboratory, the Max-Planck-Institute for Astronomy (MPIA), the Max-Planck-Institute for Astrophysics (MPA), New Mexico State University, Ohio State University, University of Pittsburgh, University of Portsmouth, Princeton University, the United States Naval Observatory, and the University of Washington.

Data Availability

The data underlying this article are publicly available at https://skyserver.sdss.org/casjobs/.

References

Ahumada, R., Allende Prieto, C., Almeida, A., et al. 2020, ApJS, 249, 3
Alonso, M. S., Lambas, D. G., Tissera, P., & Coldwell, G. 2006, MNRAS, 367, 1029
Alonso, M. S., Tissera, P. B., Coldwell, G., & Lambas, D. G. 2004, MNRAS, 352, 1081
Baldry, I. K., Glazebrook, K., Brinkmann, J., et al. 2004, ApJ, 600, 681
Barnes, J. E., & Hernquist, L. 1996, ApJ, 471, 115
Barton, E. J., Arnold, J. A., Zentner, A. R., Bullock, J. S., & Wechsler, R. H. 2007, ApJ, 671, 1538
Barton, E. J., Geller, M. J., & Kenyon, S. J. 2000, ApJ, 530, 660
Binney, J. 2004, MNRAS, 347, 1093
Birnboim, Y., & Dekel, A. 2003, MNRAS, 345, 349
Bond, J. R., Kofman, L., & Pogosyan, D. 1996, Natur, 380, 603
Bouché, N., Dekel, A., Genzel, R., et al. 2010, ApJ, 718, 1001
Brinchmann, J., Charlot, S., White, S. D. M., et al. 2004, MNRAS, 351, 1151
Cappellari, M., & Emsellem, E. 2004, PASP, 116, 138
Casertano, S., & Hut, P. 1985, ApJ, 298, 80
Conroy, C., Gunn, J. E., & White, M. 2009, ApJ, 699, 486
Cox, T. J., Jonsson, P., Primack, J. R., & Somerville, R. S. 2006, MNRAS, 373, 1013
Cox, T. J., Jonsson, P., Somerville, R. S., Primack, J. R., & Dekel, A. 2008, MNRAS, 384, 386
Das, A., Pandey, B., & Sarkar, S. 2021, JCAP, 06, 045
Das, A., Pandey, B., & Sarkar, S. 2023, RAA, 23, 025016
Das, A., Pandey, B., Sarkar, S., & Dutta, A. 2021, arXiv:2108.05874
Davé, R., Finlator, K., & Oppenheimer, B. D. 2011, MNRAS, 416, 1354
Davé, R., Finlator, K., & Oppenheimer, B. D. 2012, MNRAS, 421, 98
De Propris, R., Conselice, C. J., Liske, J., et al. 2007, ApJ, 666, 212
Dekel, A., & Birnboim, Y. 2006, MNRAS, 368, 2
Dekel, A., Sari, R., & Ceverino, D. 2009, ApJ, 703, 785
Di Matteo, P. C., Melchior, F. A.-L., & Semelin, B. 2007, A&A, 468, 61
Diaferio, A., Kauffmann, G., Colberg, J. M., & White, S. D. M. 1999, MNRAS, 307, 537
Ellison, S. L., Catinella, B., & Cortese, L. 2018, MNRAS, 478, 3447
Ellison, S. L., Patton, D. R., Simard, L., & McConnachie, A. W. 2008, AJ, 135, 1877
Ellison, S. L., Patton, D. R., Simard, L., et al. 2010, MNRAS, 407, 1514
Fakhouri, O., & Ma, C.-P. 2008, MNRAS, 386, 577
Fall, S. M., & Efstathiou, G. 1980, MNRAS, 193, 189
Förster Schreiber, N. M., & Wuyts, S. 2020, ARA&A, 58, 661
Gabor, J. M., Davé, R., Finlator, K., & Oppenheimer, B. D. 2010, MNRAS, 407, 749
Gunn, J. E., Carr, M., Rockosi, C., et al. 1998, AJ, 116, 3040
Gunn, J. E., Siegmund, W. A., Mannery, E. J., et al. 2006, AJ, 131, 2332
Gupta, A., Tran, K.-V., Cohn, J., et al. 2020, ApJ, 893, 23
Haywood, M., Lehnert, M. D., Di Matteo, P., et al. 2016, A&A, 589, A66
Heiderman, A., Jogee, S., Marinova, I., et al. 2009, ApJ, 705, 1433
Hopkins, A. M., Miller, C. J., Nichol, R. C., et al. 2003, ApJ, 599, 971
Kauffmann, G., Colberg, J. M., Diaferio, A., & White, S. D. M. 1999a, MNRAS, 303, 188
Kauffmann, G., Colberg, J. M., Diaferio, A., & White, S. D. M. 1999b, MNRAS, 307, 529
Kauffmann, G., Heckman, T. M., White, S. D. M., et al. 2003a, MNRAS, 341, 54
Kauffmann, G., Heckman, T. M., White, S. D. M., et al. 2003b, MNRAS, 341, 33
Kawata, D., & Mulchaey, J. S. 2008, ApJL, 672, L103
Knapen, J. H., & James, P. A. 2009, ApJ, 698, 1437
Lacey, C., & Cole, S. 1993, MNRAS, 262, 627
Lambas, D. G., Tissera, P. B., Alonso, M. S., & Coldwell, G. 2008, MNRAS, 346, 1189
Larson, R. B., & Tinsley, B. M. 1978, ApJ, 219, 46
Larson, R. B., Tinsley, B. M., & Caldwell, C. N. 1980, ApJ, 237, 692
Li, C., Kauffmann, G., Heckman, T. M., White, S. D. M., & Jing, Y. P. 2008, MNRAS, 385, 1915
Lilly, S. J., Carollo, C. M., Pipino, A., Renzini, A., & Peng, Y. 2013, ApJ, 772, 119
Lintott, C. J., Schawinski, K., Slosar, A., et al. 2008, MNRAS, 389, 1179
Madau, P., Ferguson, H. C., Dickinson, M. E., et al. 1996, MNRAS, 283, 1388
Martig, M., Bournaud, F., Teyssier, R., & Dekel, A. 2009, ApJ, 707, 250
Mastropietro, C., Moore, B., Mayer, L., Wadsley, J., & Stadel, J. 2005, MNRAS, 363, 509
Mihos, J. C., & Hernquist, L. 1994, ApJL, 425, L13
Mihos, J. C., & Hernquist, L. 1996, ApJ, 464, 641
Montuori, M., Di Matteo, P., Lehnert, M. D., Combes, F., & Semelin, B. 2010, A&A, 518, A56
Moreno, J., Torrey, P., Ellison, S. L., et al. 2021, MNRAS, 503, 3113
Murray, N., Quataert, E., & Thompson, T. A. 2005, ApJ, 618, 569
Nikolic, B., Cullen, H., & Alexander, P. 2004, MNRAS, 355, 874
Pan, H.-A., Lin, L., Hsieh, B.-C., et al. 2018, ApJ, 868, 132

Pandey, B. 2020, MNRAS, 499, L31
Patton, D. R., & Atfield, J. E. 2008, ApJ, 685, 235
Patton, D. R., Carlberg, R. G., Marzke, R. O., et al. 2000, ApJ, 536, 153
Patton, D. R., Ellison, S. L., Simard, L., McConnachie, A. W., & Mendel, J. T. 2011, MNRAS, 412, 591
Patton, D. R., Torrey, P., Ellison, S. L., Mendel, J. T., & Scudder, J. M. 2013, MNRAS, 433, L59
Patton, D. R., Wilson, K. D., Metrow, C. J., et al. 2020, MNRAS, 494, 4969
Perez, J., Tissera, P., & Blaizot, J. 2009, MNRAS, 397, 748
Perez, M. J., Tissera, P. B., Lambas, D. G., & Scannapieco, C. 2006, A&A, 449, 23
Planck Collaboration, Aghanim, N., Akrami, Y., et al. 2018, A&A, 641, A6
Rees, M. J., & Ostriker, J. P. 1977, MNRAS, 179, 541
Renaud, F., Bournaud, F., Kraljic, K., & Duc, P.-A. 2014, MNRAS, 442, L33
Robaina, A. R., Bell, E. F., Skelton, R. E., et al. 2009, ApJ, 704, 324
Rodríguez Montero, F., Davé, R., Wild, V., Anglés-Alcázar, D., & Narayanan, D. 2019, MNRAS, 490, 2139
Rupke, D. S. N., Kewley, L. J., & Barnes, J. E. 2010, ApJL, 710, L156
Saintonge, A., & Catinella, B. 2022, ARA&A, 60, 319
Saintonge, A., Tacconi, L. J., Fabello, S., et al. 2012, ApJ, 758, 73
Sarzi, M., Falcón-Barroso, J., Davies, R. L., et al. 2006, MNRAS, 366, 1151
Scudder, J. M., Ellison, S. L., Torrey, P., Patton, D. R., & Mendel, J. T. 2012, MNRAS, 426, 549
Silk, J. 1977, ApJ, 211, 638
Somerville, R. S., & Primack, J. R. 1999, MNRAS, 310, 1087
Springel, V., Di Matteo, T., & Hernquist, L. 2005, MNRAS, 361, 776
Strateva, I., Ivezić, Ž., Knapp, G. R., et al. 2001, AJ, 122, 1861
Strauss, M. A., Weinberg, D. H., Lupton, R. H., et al. 2002, AJ, 124, 1810
Thorp, M. D., Ellison, S. L., Pan, H.-A., et al. 2022, MNRAS, 516, 1462
Tissera, P. B. 2000, ApJ, 534, 636
Tissera, P. B., Domínguez-Tenreiro, R., Scannapieco, C., & Sáiz, A. 2002, MNRAS, 333, 327
Toomre, A., & Toomre, J. 1972, ApJ, 178, 623
Torrey, P., Cox, T. J., Kewley, L., & Hernquist, L. 2012, ApJ, 746, 108
Tran, K.-V. H., Papovich, C., Saintonge, A., et al. 2010, ApJL, 719, L126
van den Bosch, F. C., Aquino, D., Yang, X., et al. 2008, MNRAS, 387, 79
Violino, G., Ellison, S. L., Sargent, M., et al. 2018, MNRAS, 476, 2591
White, S. D. M., & Rees, M. J. 1978, MNRAS, 183, 341
Willett, K. W., Lintott, C. J., Bamford, S. P., et al. 2013, MNRAS, 435, 2835
Woods, D. F., & Geller, M. J. 2007, AJ, 134, 527
Woods, D. F., Geller, M. J., & Barton, E. J. 2006, AJ, 132, 197
Woods, D. F., Geller, M. J., Kurtz, M. J., et al. 2010, AJ, 139, 1857
Wright, R. J., del P. Lagos, C., Power, C., et al. 2022, MNRAS, 516, 2891
York, D. G., Adelman, J., Anderson, J. E., Jr, et al. 2000, AJ, 120, 1579